
CAUSAL DISCOVERY-DRIVEN CHANGE POINT DETECTION IN TIME SERIES

Shanyun Gao
Purdue University
gao565@purdue.edu

Raghavendra Addanki
Adobe Research
raddanki@adobe.com

Tong Yu
Adobe Research
tyu@adobe.com

Ryan A. Rossi
Adobe Research
ryrossi@adobe.com

Murat Kocaoglu
Purdue University
mkocaoglu@purdue.edu

July 11, 2024

ABSTRACT

Change point detection in time series seeks to identify times when the probability distribution of time series changes. It is widely applied in many areas, such as human-activity sensing and medical science. In the context of multivariate time series, this typically involves examining the joint distribution of high-dimensional data: If any one variable changes, the whole time series is assumed to have changed. However, in practical applications, we may be interested only in certain components of the time series, exploring abrupt changes in their distributions in the presence of other time series. Here, assuming an underlying structural causal model that governs the time-series data generation, we address this problem by proposing a two-stage non-parametric algorithm that first learns parts of the causal structure through constraint-based discovery methods. The algorithm then uses conditional relative Pearson divergence estimation to identify the change points. The conditional relative Pearson divergence quantifies the distribution disparity between consecutive segments in the time series, while the causal discovery method enables a focus on the causal mechanism, facilitating access to independent and identically distributed (IID) samples. Theoretically, the typical assumption of samples being IID in conventional change point detection methods can be relaxed based on the Causal Markov Condition. Through experiments on both synthetic and real-world datasets, we validate the correctness and utility of our approach.

1 Introduction

Change point analysis aims to detect distribution shifts in observational time series data. This topic has been explored extensively and is popular in many areas, such as human activity analysis Brahim-Belhouari and Bermak [2004], Cleland et al. [2014], image analysis Radke et al. [2005] and financial markets Talih and Hengartner [2005].

Various change point detection methods are chosen based on the compatibility between the statistical feature shifts they detect and the characteristics of the data.

Likelihood ratio methods compare the probability density of two consecutive intervals of the time series data and the significant difference in the probability density implies the change point. One representative estimator is the relative unconstrained least-squares importance fitting (RuLSIF) in Yamada et al. [2013] and Liu et al. [2013].

Kernel-based methods in Harchaoui et al. [2008] and Harchaoui et al. [2009] utilize kernel-based test statistics to test the homogeneity of sliding windows in time series data. Other methods include Probabilistic methods, Graph-based methods, clustering methods and Subspace modeling. See Chib [1998], Friedman and Rafsky [1979], Keogh et al. [2001] and Itoh and Kurths [2010], respectively. See Aminikhanghahi and Cook [2017] for a survey.

However, these existing methods have two main limitations. Firstly, for multivariate time series, the target features are generated from the joint distribution, which is typically high-dimensional. Ignoring the impact of high-dimensional data, this problem remains fundamental: if a change occurs in only one univariate time series, it will affect the joint feature of the entire multivariate time series. With multiple change point estimators, which estimator corresponds to which univariate time series is unknown. In practice, considering a bivariate time series, such as daily temperature and ice cream sales, or monthly GDP and stock prices, the change points across the whole series is less interesting than the change point of ice cream sales and stock prices, given the information from temperature and GDP. Applying the detection method to each univariate time series individually will lose information, especially if there are strong correlations among the component time series.

Secondly, many existing methods, including probability density ratio methods, some probabilistic methods, kernel-based methods, and graph-based methods, require independent and identically distributed (IID) samples Aminikhanghahi and Cook [2017], Harchaoui et al. [2008], Liu et al. [2013], Saggioro et al. [2020]. Although many of these methods are robust to non-IID samples in simulated data Liu et al. [2013], they lack theoretical guarantees, which are needed for trustworthy deployment of these algorithms in the real world, especially in safety-critical applications Liu et al. [2018].

To address these limitations, we propose a novel change point detection algorithm that integrates change point detection with causal discovery. Our algorithm is motivated by the following two considerations.

First, causal structure helps us obtain a more fine-grained look at the joint distribution by disentangling the causal mechanism of each component in the time series. Second, relying on the Causal Markov Condition assumption in the Structural Causal Model (SCM) framework of Pearl [2009], the correlated samples become independent and identically distributed (IID) when conditioned on their causal parents. This observation has been successfully used earlier in causal discovery from stationary time-series data Runge [2018]. In this context, change point detection aims to identify shifts in the causal mechanism, specifically, the conditional distribution of the target variable given its parents.

In this paper, we summarize our main contributions as follows:

- We propose a novel non-parametric algorithm aiming at detecting the change point in causal mechanisms for discrete-valued time series data assuming an underlying *Causal-Shift* SCM without imposing any constraints on the causal mechanisms or the data distributions. Our algorithm Causal-RuLSIF, systematically uses the RuLSIF estimator for detecting change points, originally introduced in Yamada et al. [2013] and Liu et al. [2013], integrating the PCMCI algorithm for causal discovery in Runge et al. [2019].
- We validate our method with synthetic simulations on both *soft mechanism change* and *hard mechanism change* time series, showing that our method can correctly detect the change points with high probability and hence learn the causal mechanism of the synthetic time series. We also employ our method in an air pollution application.

2 Related Work

Depending on the underlying goal, our algorithm can be used to solve either a change point detection problem or a causal discovery problem. Hence, there are two different directions of the related work.

Regarding the change point detection problems, one representative likelihood ratio estimator used to detect the distribution shifts is RuLSIF, which was first proposed for distribution comparison with IID samples in Yamada et al. [2013] and then has been verified as a useful method for time series data in Liu et al. [2013]. As discussed in the instruction section, such existing methods concentrate on joint features associated with all time series, with many assuming IID samples.

As for the causal discovery methods, numerous efforts have been made recently to extend constraint-based algorithms to accommodate stationary time series data. One representative method is PCMCI in Runge et al. [2019]. Non-stationary temporal data is more challenging in causal discovery since data statistics are time-variant, and it is unreasonable to expect that the underlying causal structure will remain constant. Many of the causal discovery methods with non-stationary time series assume a parametric model, such as the vector autoregressive model in Gong et al. [2015] and Malinsky and Spirtes [2019]; linear and non-linear state-space model in Huang et al. [2019]; linear causal relationship in Saggioro et al. [2020]. A non-parametric algorithm, named CD-NOD in Huang et al. [2020] assumes a smooth change in the causal mechanism across the time index instead of a sudden change. Fujiwara et al. [2023] proposed an algorithm JIT-LiNGAM to obtain a local approximated linear causal model combining algorithm LiNGAM and JIT framework for non-linear and non-stationary data. In Gao et al. [2023], the underlying causal mechanism of each time series is assumed to change sequentially and periodically.

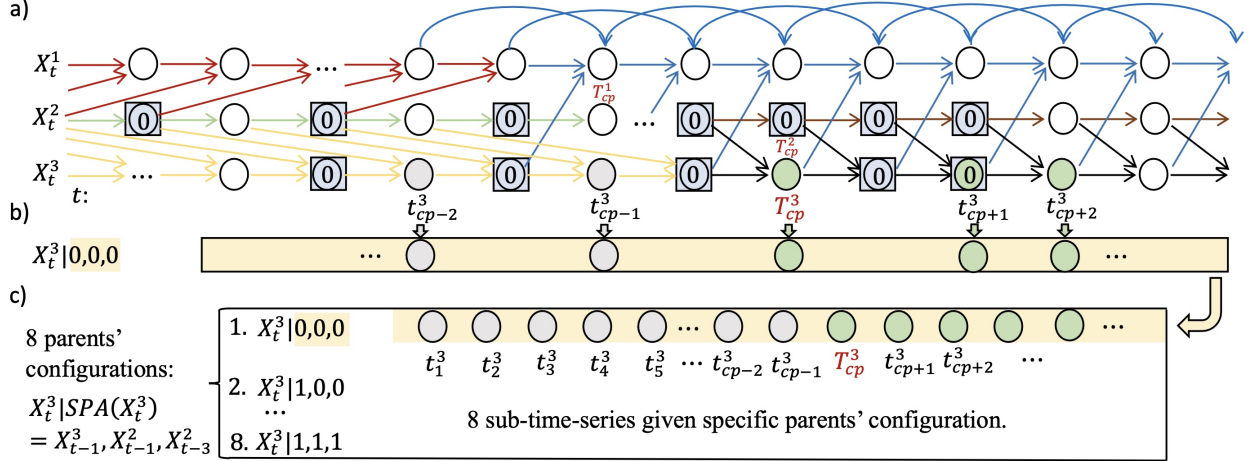


Figure 1: An illustration of generating time series segments in Causal-RuLSIF. a). Causal graph illustrating a 3-variate binary time series $V = \{\mathbf{X}^1, \mathbf{X}^2, \mathbf{X}^3\}$ with a *Mechanism-Shift* SCM with $c^1 = c^2 = c^3 = 1$, indicating the presence of one change points in each univariate time series. It is important to note that the location of change points for different univariate time series may vary. For instance, the first change point for X^2 is denoted as T_{cp}^1 , whereas the first change point for X^1 is denoted as T_{cp}^2 , and T_{cp}^1 is not equal to T_{cp}^2 . The different color edges represent different causal mechanisms. E.g., for \mathbf{X}^1 , the causal mechanism represented by the red edges transitions to a different causal mechanism indicated by the blue edges at time point T_{cp}^1 . No constraints on the causal mechanisms, e.g., for \mathbf{X}^1 , the two causal mechanisms before and after the change point T_{cp}^1 are different in both the parent sets and the deterministic function $f_{1,t}(\cdot)$; we refer to this situation as *soft mechanism change*. For \mathbf{X}^2 , the two causal mechanisms are only different in $f_{2,t}(\cdot)$ while the parent set remains the same; we refer to this situation as *hard mechanism change*. b). Construction of one time series segment for \mathbf{X}^3 . With $PA(X_{t_1 < T_{cp}^3}^3) = \{X_{t-1}^3, X_{t-3}^3\}$, $PA(X_{t_2 \geq T_{cp}^3}^3) = \{X_{t-1}^3, X_{t-1}^2\}$, we have $SPA(X_t^3) = PA(X_{t_1 < T_{cp}^3}^3) \cup PA(X_{t_2 \geq T_{cp}^3}^3)$. Given one specific configuration of $SPA(X_t^3)$, $spa(X_t^3) = \{X_{t-1}^3 = 0, X_{t-1}^2 = 0, X_{t-3}^2 = 0\}$, we need to collect all variable $X_t^3 \in \mathbf{X}^3$ whose parent variables are equal to 0 to form the first time series segment of \mathbf{X}^3 . c). Collection of 8 time series segments for \mathbf{X}^3 as there are total 8 parents' configurations.

To the best of our knowledge, no other non-parametric change point detection models can detect the causal mechanism shifts. On the other hand, our change point detection algorithm, when combined with a post-processing causal discovery step, is, as far as we know, the first non-parametric method that can learn causal structure from non-stationary time-series data without assuming periodicity while also accommodating sudden shifts in causal mechanisms.

3 Causal-RuLSIF: Detecting Change Point in a Causal Time Series

In this section, we describe the framework and problem formulation for change point detection in a causal time series.

3.1 Preliminaries

Let $\mathcal{G}(V, E)$ denote the underlying causal graph, and the set of all incoming neighbors for each variable $X \in V$ is defined as the parent set, denoted by $PA(X)$. For any $X, Y \in V$ and $S \subset V$, we denote the conditional independence: X is independent of Y conditioned on S , by $X \perp\!\!\!\perp Y \mid S$.

For simplicity, let's define sets: $[b] := \{1, 2, \dots, b\}$ and $[a, b] := \{a, a+1, \dots, b\}$, where $a, b \in \mathbb{N}$. Let $X_t^j \in \mathbb{R}$ denote the variable of j th *component* time series at time t ; $\mathbf{X}^j = \{X_t^j\}_{t \in [T]} \in \mathbb{R}^T$ denote a univariate time series which is a component in time series and $\mathbf{X}_t = \{X_t^j\}_{j \in [n]} \in \mathbb{R}^n$ denote a slice of all variables at time point t . $V = \{\mathbf{X}^j\}_{j \in [n]} = \{\mathbf{X}_t\}_{t \in [T]} \in \mathbb{R}^{n \times T}$ denotes a n -variate time series. By default, we assume $n > 1$ and hence

$\mathbf{X}^j \subsetneq V$, and $p(V) \neq 0$, where $p(\cdot)$ denotes the probability. For discrete-valued time series V , we assume that the domain set of each component $\mathbf{X}^j \subsetneq V$, denoted by $D = \{d_1, \dots, d_s\}$ is the same, i.e., $X_t^j \in D \forall j \in [n], t \in [T]$.

As $\text{PA}(X_t^j)$ represents a set containing random variables, $\text{pa}(X_t^j)$ refers to one specific configuration. Consider $\text{PA}(X_t^j) = \{X_{t_1}^{i_1}, X_{t_2}^{i_2}, \dots\}$ where $1 \leq i_1 \leq i_2 \leq \dots \leq n$ and $1 \leq t_1 \leq t_2 \leq \dots \leq T$. E.g., $\text{pa}(X) = \{1, 0, 1, 2, \dots\}$ corresponds to a particular configuration (or instantiation). We assume that the configuration set is ordered in the ascending order of the parent set $\{X_{t_1}^{i_1}, X_{t_2}^{i_2}, \dots\}$, prioritizing the variable index over the time index. We begin by defining the Structural Causal Models (SCM) that capture our setting.

Definition 3.1 (Non-Stationary SCM [Gao et al., 2023]). *A Non-Stationary SCM is a tuple $\mathcal{M} = \langle V, \mathcal{F}, \mathcal{E}, \mathbb{P} \rangle$ where there exists a $\tau_{\max} \in \mathbb{N}^+$, defined as: $\tau_{\max} := \max_{\tau} \{\tau : X_{t-\tau}^i \in \text{PA}(X_t^j), i, j \in [n]\}$, such that each variable $X_{t>\tau_{\max}}^j \in V$ is a deterministic function of its parent set $\text{PA}(X_{t>\tau_{\max}}^j) \in V$ and an unobserved (exogenous) variable $\epsilon_{t>\tau_{\max}}^j \in \mathcal{E}$:*

$$X_t^j = f_{j,t}(\text{PA}(X_t^j), \epsilon_t^j), \quad j \in [n], t \in [\tau_{\max} + 1, T], \quad (1)$$

and there exist at least two different time points $t_0, t_1 \in [\tau_{\max} + 1, T]$ satisfying

$$f_{j,t_0} \neq f_{j,t_1}, \quad \exists j \in [n], \{t_0, t_1\} \subset [\tau_{\max} + 1, T]. \quad (2)$$

where $f_{j,t}, f_{j,t_0}, f_{j,t_1} \in \mathcal{F}$ and $\{\epsilon_t^j\}_{t \in [T]}$ are jointly independent with probability measure \mathbb{P} . Observe that τ_{\max} is the finite maximal lag in terms of the causal graph \mathcal{G} .

Definition 3.2 (Mechanism-Shift SCM). *A Mechanism-Shift SCM is a Non-Stationary SCM that additionally satisfies the following conditions. For each $j \in [n]$, there exists an ascending sequence of time points $\{T_1^j, T_2^j, \dots, T_{c^j}^j\}$ with $c^j \in \mathbb{N}^+$, $\tau_{\max} < T_1^j < \dots < T_{c^j}^j < T$ such that:*

$$a) f_{j,t_1} = f_{j,t_2}, \text{ if } \exists c \in [c^j] \text{ s.t. } t_1, t_2 \in [T_c^j, T_{c+1}^j - 1]; \quad (3)$$

$$b) f_{j,t_1} \neq f_{j,t_2}, \text{ if } \exists c \in [c^j] \text{ s.t. } T_{c-1}^j \leq t_1 < T_c^j \leq t_2 < T_{c+1}^j; \quad (4)$$

$$c) \text{PA}(X_{t_1}^j) = \{X_{s+(t_1-t_2)}^i : X_s^i \in \text{PA}(X_{t_2}^j), i \in [n]\}, \quad (5)$$

$$\text{if } \exists c \in [c^j] \text{ s.t. } t_1, t_2 \in [T_c^j, T_{c+1}^j - 1]; \quad (6)$$

$$d) \epsilon_t^j, \epsilon_{t+N\omega}^j \text{ are i.i.d. } \forall t \in [T]. \quad (7)$$

are satisfied for all $t_1, t_2 \in [\tau_{\max} + 1, T]$. This indicates that within the univariate time series \mathbf{X}^j in V , there is a finite number of change points represented by c^j . The variables in \mathbf{X}^j before and after a specific change point should exhibit distinct causal mechanisms without intersecting other change points. An instance of this model is depicted in Fig. 1a).

Our goal is to detect the change points of the causal mechanisms, and if necessary any causal relations that might be helpful.

Definition 3.3 (Illusory Parent Sets). *For a univariate time series $\mathbf{X}^j \in V$ with Mechanism-Shift SCM having change points set $\{T_1^j, T_2^j, \dots, T_{c^j}^j\}$ with $c^j \in \mathbb{N}^+$, $\tau_{\max} < T_1^j < \dots < T_{c^j}^j < T$, parent set index $\text{pInd}_{k \in [c^j+1]}$ is defined as:*

$$\text{pInd}_k^j := \{(\tau_i, y_i)\}_{i \in [n]}, \text{ given } \text{PA}(X_t^j) = \{X_{t-\tau_1}^{y_1}, X_{t-\tau_2}^{y_2}, \dots, X_{t-\tau_n}^{y_n}\}, \forall t \in [T_{k-1}^j, T_k^j] \quad (8)$$

where $n = |\text{PA}(X_t^j)|$, τ_i is the time lag and y_i is the variable index; set $T_0^j = \tau_{\max}$ and $T_{c^j+1}^j = T$. Given pInd_k , Illusory Parent Sets are defined as:

$$\text{PA}_k(X_t^j) = \{X_{t-\tau_i}^{y_i} : (\tau_i, y_i) \in \text{pInd}_k^j\}, \quad \forall k \in \{k : t \notin [T_{k-1}^j, T_k^j]\} \quad (9)$$

In essence, the illusory parent sets of X_t^j are time-shifted versions of the parent sets of other variables in \mathbf{X}^j that have different causal mechanisms than X_t^j across change points. These sets are a generalization of a notion described in Gao et al. [2023]. $\text{PA}_k(X_t^j)$ can also be extended to encompass the true parent set of X_t^j , as: $\text{PA}_k(X_t^j) := \text{PA}(X_t^j)$, $\forall t \in [T_{k-1}^j, T_k^j]$. Further, we define the union parent set as:

$$\text{SPA}(X_t^j) := \cup_{k \in [c^j+1]} \text{PA}_k(X_t^j), \quad t \in [\tau_{\max} + 1, T] \quad (10)$$

E.g., in Fig. 1a), $\text{PA}(X_t^1) = \{X_{t-1}^1, X_{t-2}^2\}$ with $t < t_{cp}^1$ and $\text{PA}(X_t^1) = \{X_{t-1}^1, X_{t-2}^1, X_{t-1}^3\}$ with $t \geq t_{cp}^1$. As only one change point of \mathbf{X}^j with $c^1 = 1$ exists, we have two illusory parent sets with index $k \in [c^1 + 1]$. More specifically, the two illusory parent sets of \mathbf{X}^1 are $\text{PA}_1(X_t^1) = \{X_{t-1}^1, X_{t-2}^2\}$ and $\text{PA}_2(X_t^1) = \{X_{t-1}^1, X_{t-2}^1, X_{t-1}^3\}$.

Definition 3.4 (Time Series Segments). For a univariate discrete-valued time series $\mathbf{X}^j \in V$ with Mechanism-Shift SCM having change points set $\{T_1^j, T_2^j, \dots, T_{c^j}^j\}$ with $c^j \in \mathbb{N}^+$, $\tau_{\max} < T_1^j < \dots < T_{c^j}^j < T$, and finite domain set $D = \{d_1, d_2, \dots, d_s\}$, the Time Series Segments are a collection of non-overlapping non-empty subsets $\{X^j(\Lambda)\}_{\Lambda \in [s^{|\text{SPA}(X_t^j)}]}$ such that:

$$X^j(\Lambda) := \{X_t^j : t \in [\tau_{\max} + 1, T], \text{pa}(X_t^j) = \Sigma_\Lambda^j\}, \text{ where } \Lambda \in [s^{|\text{SPA}(X_t^j)}]. \quad (11)$$

Here, Σ represents the configuration matrix of $\text{SPA}(X_t^j)$, where each row corresponds to one specific configuration of $\text{SPA}(X_t^j)$. Λ denotes the row index of Σ . As the domain size is $|D| = s$, the number of rows in Σ is $s^{|\text{SPA}(X_t^j)}|$. Based on the above definition, we can observe that:

$$\bigcup_{\Lambda \in [s^{|\text{SPA}(X_t^j)}]} \{X^j(\Lambda)\} = \mathbf{X}^j \text{ and } \bigcap_{\Lambda_1 \neq \Lambda_2} \{X^j(\Lambda)\} = \emptyset. \quad (12)$$

In summary, the Time Series Segments $\{X^j(\Lambda)\}$ partition \mathbf{X}^j into multiple non-overlapping, non-empty sub-time series, conditioned on the configurations of the union parent set $\text{SPA}(\mathbf{X}^j)$. Variables X_t^j within the same Time Series Segments $\mathbf{X}^j(\Lambda)$ share identical configurations of the union parent set (See Appendix A.1.1 for an example).

RuLSIF: Robust Distributional Distance Estimation. Given two distributions $p(\cdot)$ and $p'(\cdot)$ defined over the same support, there exists many metrics measuring the distance between them. In Yamada et al. [2013], the authors proposed a method named RuLSIF, with an α -relative divergence estimation $r_\alpha(x)$ and a corresponding metric, α -relative Pearson Divergence PE_α defined as following:

$$r_\alpha(x) := \frac{p(x)}{(1 - \alpha)p(x) + \alpha p'(x)} := \frac{p(x)}{q_\alpha(x)} \text{ and } PE_\alpha := \frac{1}{2} \mathbb{E}_{x \sim q_\alpha} [(r_\alpha(x) - 1)^2] \quad (13)$$

where α is a parameter used to bound the value of $r_\alpha(x)$.

In our work, we revised the above definition for better applicability in the time series, incorporating a sliding window index i . Denote the sliding windows as W_i . Instead of having two fixed sets of IID samples, we now collect samples dynamically. In sliding windows where a change point occurs in the second half, the samples in that second half window are drawn from a mixture distribution represented by $(1 - \beta_i)p(x) + \beta_i p'(x)$, where β_i indicates the proportion of samples in the second half derived from $p'(x)$. Based on this, the dynamic density ratio and the corresponding PE divergence score are defined as follows:

$$r_{\alpha\beta_i}(x) := \frac{p(x)}{(1 - \alpha\beta_i)p(x) + \alpha\beta_i p'(x)} := \frac{p(x)}{q_{\alpha\beta_i}(x)} \text{ and } PE_{\alpha\beta_i} := \frac{1}{2} \mathbb{E}_{x \sim q_{\alpha\beta_i}} [(r_{\alpha\beta_i}(x) - 1)^2] \quad (14)$$

Assumptions. We highlight the key assumptions that we make: (1) At most one change point for any univariate time series, and a (2) lower bound on the Pearson Divergence. The first assumption ensures that multiple change points do not have a cancellation effect making it difficult to identify the change point, while the second assumption is commonly used in many standard distributional distance estimation papers in the finite sample, discrete settings.

The formalization of these two assumptions is provided in Appendix A.1.3, where other assumptions that are known in prior works can also be found.

4 Causal-RuLSIF Algorithm

In this section, we first present an algorithm called Causal-RuLSIF. We also establish the correctness of Causal-RuLSIF to estimate the change point within a confidence interval accurately.

Overview of Algorithm 1 Causal-RuLSIF: The values of the parameters n_w , n_{st} and α are set in the beginning. Each component \mathbf{X}^j where $j \in [n]$ is analyzed sequentially. Using PCMCI Runge et al. [2019], we obtain a superset of parents for each variable $X_t^j \in \mathbf{X}^j$ denoted by $\text{SPA}(X_t^j)$ (line 2). To have balanced samples required in Theorem A.1, we apply PCMCI to non-overlapping consecutive intervals and take the union of the obtained edges. Based on the parents' configurations of $\text{SPA}(X_t^j)$, Time Series Segments $\{X^j(\Lambda)\}$ are constructed. After using RuLSIF Yamada et al. [2013] and Liu et al. [2013] on sliding windows over $\{X^j(\Lambda)\}$, we obtain the divergence series denoted by $\{\widehat{PE}_{\alpha\beta_i}^{j,\Lambda}\}$ (line 7-8). Note that the number of Time Series Segments should equal the number of divergence series, as each Time Series Segments will have a divergence series. Across all divergence series for \mathbf{X}^j , the change point

Algorithm 1 Causal-RuLSIF

- 1: **Input:** A n -variate time series $V = (\mathbf{X}^1, \mathbf{X}^2, \dots, \mathbf{X}^n)$ with domain set $D = \{d_1, \dots, d_s\}$. Set appropriate $\tau_{\text{ub}}, n_{\text{w}}, n_{\text{st}}$ and α .
 - 2: A superset of the parent set is obtained using PCMCI with τ_{ub} and denote it by $\widehat{\text{SPA}}(X_t^j) \forall j, t$.
 - 3: **for** \mathbf{X}^j where $j \in [n]$ **do**
 - 4: $\widehat{\text{PA}}(X_t^j) \leftarrow \widehat{\text{SPA}}(X_t^j)$
 - 5: Construct the Time Series Segments $\{X^j(\Lambda)\}$ based on parents' configurations of $\widehat{\text{SPA}}(X_t^j)$.
 - 6: **for** $X^j(\Lambda)$ where $\Lambda \in [s^{|\widehat{\text{SPA}}(X_t^j)|}]$ **do**
 - 7: Store divergence score series $\{\widehat{PE}_{\alpha\beta_i}^{j,\Lambda}\}$ with RuLSIF on sliding windows shifting over $X^j(\Lambda)$ where $i \in [\lfloor \frac{|T_{\text{sub}}| - 2n_{\text{w}}}{n_{\text{st}}} \rfloor + 1]$ and $T_{\text{sub}} = |X^j(\Lambda)|$.
 - 8: **end for**
 - 9: $\widehat{\Lambda} \leftarrow \arg_{\Lambda} \max_{i,\Lambda} \widehat{PE}_{\alpha\beta_i}^{j,\Lambda}$ ▷ Pick the Λ th Time Series Segments whose maximum value over i is maximum.
 - 10: $\widehat{T}_c^j \leftarrow \arg_i \max \widehat{PE}_{\alpha\beta_i}^{j,\widehat{\Lambda}}$ ▷ Pick the i th window index with maximum PE score on $X^j(\widehat{\Lambda})$.
 - 11: Project \widehat{T}_c^j , where $j \in [n]$, back to the original time series \mathbf{X}^j with $\widetilde{T}_c^j = \frac{1}{2}(t_{\widehat{T}_c^j} + t_{\widehat{T}_c^j+1})$, where $t_{\widehat{T}_c^j}$ is the time index in \mathbf{X} corresponding to the window index \widehat{T}_c^j in $X^j(\widehat{\Lambda})$.
 - 12: Consider $X_{t-\tau}^j \in \widehat{\text{PA}}(X_t^j)$. Remove $X_{t-\tau}^j$ from $\widehat{\text{PA}}(X_t^j)$ using PCMCI if $X_{t-\tau}^j \perp\!\!\!\perp X_t^j \mid (\widehat{\text{SPA}}(X_t^j) \cup \widehat{\text{SPA}}(X_{t-\tau}^j)) \setminus X_{t-\tau}^j$ on samples $\{X_t^j\}_{t < \widetilde{T}_c^j}$ and $\{X_t^j\}_{t \geq \widetilde{T}_c^j}$ respectively.
 - 13: **end for**
 - 14: **return** \widetilde{T}_c^j and $\widehat{\text{PA}}(X_t^j) \forall j, t$.
-

estimator \widehat{T}_c^j is the window index that *maximizes the PE divergence* of $\widehat{PE}_{\alpha\beta_i}^{j,\Lambda}$, based on all Time Series Segments (line 9-10). Since \widehat{T}_c^j is the window index in Time Series Segments and not the original time index in \mathbf{X} , it should be projected back to \mathbf{X} . The final change point estimator for \mathbf{X} is then obtained and denoted as \widetilde{T}_c^j (line 11). After obtaining an accurate estimator \widehat{T}_c^j proved in Theorem 4.2, one may optionally run PCMCI on samples X_t^j before and after the change point \widetilde{T}_c^j , respectively, to fully learn the underlying causal graph.

4.1 Theoretical Guarantees

Theorem 4.1 establishes that if the window W_i only contains samples from a single conditional distribution, meaning there is no change point included in this window, the estimated relative Pearson Divergence $\widehat{PE}_{\alpha\beta_i}$ is close to zero with high probability. Theorem 4.2 provides a confidence interval for the change point estimator \widehat{T}_c^j . All the missing details are provided in Appendix A.2.

Theorem 4.1. *Let $\widehat{PE}_{\alpha\beta_i}$ be the estimated PE series for one Time Series Segments $X^j(\Lambda) \subsetneq \mathbf{X}^j \subsetneq V$. Under certain assumptions, we have that $\forall i \in \{i : in_{\text{st}} + 2n_{\text{w}} - 1 < T_c\}$*

$$\Pr(\max_i |\widehat{PE}_{\alpha\beta_i}| < o_p(1)) > 1 - \frac{a_{\text{w}} - 2}{b_{\text{st}} \log T_{\text{sub}}} - \frac{a_{\text{w}}}{T_{\text{sub}}},$$

where $b_{\text{st}} = \lfloor \frac{\log T_{\text{sub}}}{n_{\text{st}}} \rfloor$, $a_{\text{w}} = \lceil \frac{T_{\text{sub}}}{n_{\text{w}}} \rceil$ and T_{sub} as defined in Algorithm 1.

The window index i satisfying $in_{\text{st}} + 2n_{\text{w}} - 1 < T_c$ guarantees that all the samples in W_i are collected from the same distribution. Theorem 4.1 states that the maximum estimated PE series obtained from such windows are bounded by any positive constant with probability $1 - \frac{a_{\text{w}} - 2}{b_{\text{st}} \log T_{\text{sub}}} - \frac{a_{\text{w}}}{T_{\text{sub}}}$ if n_{w} are larger than some threshold.

Theorem 4.2. *Let $\widehat{PE}_{\alpha\beta_i}$ be the estimated PE series for one Time Series Segments $X^j(\Lambda) \subsetneq \mathbf{X}^j \subsetneq V$ and T_c^j denote the true change point in this Time Series Segments. \widehat{T}_c^j denotes the estimator of T_c^j obtained by:*

$$\widehat{T}_c^j = \arg_i \max \widehat{PE}_{\alpha\beta_i} \tag{15}$$

Under certain assumptions, we have that given large enough $n_{\text{w}}, \forall i \in [\tau_{\text{max}} + 1, T]$

$$\Pr(|\widehat{T}_c^j - T_c^j| < 2n_{\text{w}}) > \left(1 - \frac{a_{\text{w}} - 2}{b_{\text{st}} \log T_{\text{sub}}} - \frac{a_{\text{w}}}{T_{\text{sub}}}\right) \left(1 - \frac{1}{n_{\text{w}}}\right), \tag{16}$$

where $b_{\text{st}} = \lfloor \frac{\log T_{\text{sub}}}{n_{\text{st}}} \rfloor$, $a_{\text{w}} = \lceil \frac{T_{\text{sub}}}{n_{\text{w}}} \rceil$, and T_{sub} as defined in Algorithm 1

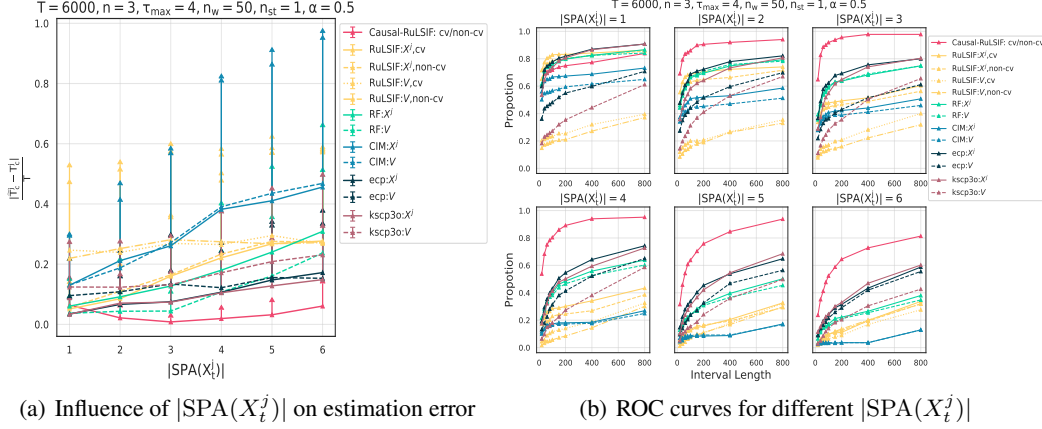


Figure 2: Causal-RuLSIF is tested on 3-multivariate time series with $T = 6000, \tau_{\max} = 4, n_w = 50, n_{st} = 1$ with *soft mechanism change*. Every line with a different color corresponds to a different algorithm and different linestyle corresponds to a different setting. X^j in the legend means the algorithm is applied to each univariate time series while V means the algorithm is used for the whole n -variate time series V . Every marker corresponds to the average accuracy rate or average running time over 100 random trials. The error bar represents the standard error for the averaged statistics. a) Influence of $|\text{SPA}(X_t^j)|$ on estimation error $\frac{|\tilde{T}_c^j - T_c^j|}{T}$. b) ROC curves for different $|\text{SPA}(X_t^j)|$.

The change point estimator has an estimation error smaller than the total window size with a known probability.

5 Experiments

In this section, we provide an empirical evaluation of our approaches against existing approaches on synthetic and real-world datasets.

5.1 Simulations on binary multivariate time series

To validate the correctness and effectiveness of our algorithm, we perform a series of experiments on binary-valued time series dataset. In this section, we have five baseline algorithms, including RuLSIF algorithm in Liu et al. [2013], traditional method change in mean (CIM) in Vostrikova [1981], changeforest algorithm (RF) in Londschieen et al. [2023], ecp algorithm in James and Matteson [2013] and kscp3o algorithm in Zhang et al. [2017]. The RuLSIF algorithm is executed using Matlab code provided by the authors. CIM and RF are implemented through the changeforest Python package. Both ecp and kscp3o are sourced from the ecp R package. All experimental code is included in the supplementary files.

The details of synthetic binary time series generation can be found in the Appendix B.

We have two methods to evaluate the performance of the algorithms. The first method is to calculate the estimation error using $\frac{|\tilde{T}_c^j - T_c^j|}{T}$. The second method is to construct an ROC curve by setting an interval length, denoted as $2Q$. With the change point estimator \tilde{T}_c and interval length Q , we increment a counter by 1 if the true change point T_c^j falls within the interval $[\tilde{T}_c^j - Q, \tilde{T}_c^j + Q]$. This count is then averaged over the total number of univariate time series in the 100 random trials. This is a common metric for measuring the performance of the change point detection algorithm, as described in Liu et al. [2013] and Harchaoui et al. [2008].

Please note that in the RuLSIF method, the kernel width σ and the regularization parameter in the kernel function are typically chosen using cross-validation, as outlined in Liu et al. [2013] and Harchaoui et al. [2008]. This approach is justified, as high-dimensional data can render these parameters more sensitive. However, for binary time series, cross-validation may not be necessary when applying our method, Causal-RuLSIF. One possible reason is that our algorithm avoids the complexities associated with high-dimensional data V by focusing on the analysis of one-dimensional time series segments $X^j(\lambda) \subsetneq V$. As shown in Fig.2(a) and Fig.2(b), the red line represents our algorithm. With or without the cross-validation technique does not influence its performance. For RuLSIF, the cross-validation (cv) and no cross-validation (non-cv) does not overlap.

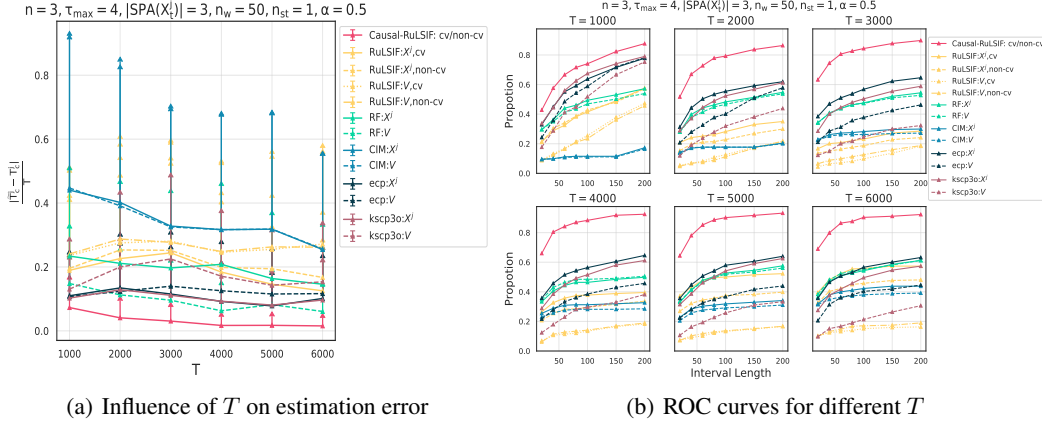


Figure 3: Causal-RuLSIF is tested on 3-multivariate time series with $|\text{SPA}(X_t^j)| = 3$, $\tau_{max} = 4$, $n_w = 50$, $n_{st} = 1$ with *soft mechanism change*. Every line with a different color corresponds to a different algorithm and different linestyle corresponds to a different setting. X^j in the legend means the algorithm is applied to each univariate time series while V means the algorithm is used for the whole n -variate time series V . Every marker corresponds to the average accuracy rate or average running time over 100 random trials. The error bar represents the standard error for the averaged statistics. a) Influence of T on estimation error $\frac{|\tilde{T}_c^j - T_c^j|}{T}$. b) ROC curves for different T .

For all the baselines, we either apply them to the entire n -variate time series or to each component \mathbf{X}^j . In the former scenario, multiple change point estimations are expected, making it difficult to determine which corresponds to which univariate time series. For the RuLSIF method, we select the estimations with the top n change scores and randomly assign them to each univariate time series. Regarding RF, CIM, ecp, and kscp3o, even if the optimal estimations are selected when T_c^j is known, their performance does not surpass ours. In the case of *RF* and *CIM*, the change point detection relies on the significance of certain statistics. If these methods fail to detect any change point, we set the estimated change point to T .

From Fig.2(a) and Fig.2(b), Causal-RuLSIF is not optimal when $|\text{SPA}(X_t^j)| = 1$. In this scenario, each variable X_t^j only receives an incoming edge from its only parent X_{t-1}^j , indicating no correlation among different time series. Therefore, it's reasonable for some baselines to exhibit better performance when applied individually to each time series. However, when $|\text{SPA}(X_t^j)| > 1$, our algorithm outperforms others, as it focuses on shifts in causal mechanisms given other time series. The performance of Causal-RuLSIF decreases as $|\text{SPA}(X_t^j)|$ increases because the effective sample size decreases with the number of parent configurations, which is $2^{|\text{SPA}(X_t^j)|}$ for binary time series.

Additional experiments on *hard mechanism change*, the impact of T , the relative location of T_c^1 and T_c^2 , and runtime analysis are provided in Appendix C.

From Fig.3(a) and Fig.3(b), it is evident that increasing the length T of the time series V enhances the performance of Causal-RuLSIF, thus practically validating the consistency of the algorithm.

5.2 Case Study

Here, we construct an experiment with a real-world air pollution dataset. This dataset monitors the amount of PM_{10} (coarse particles with a diameter between 2.5 and 10 micrometers) in the air. The 3-variate time series data records the hourly concentration of PM_{10} across three counties in California—Fresno, Mono and Monterey—from Jan to June 2023. There are a total of 4305 samples. Let \mathbf{X}^{Fr} , \mathbf{X}^{Mono} and \mathbf{X}^{Mont} denote the indicators of PM_{10} exceeding 10 across the three counties.

Using Causal-RuLSIF, the change point estimators \tilde{T}_c^j for each \mathbf{X}^j where $j \in [4]$ are shown in the Table 1, along with the parent sets before and after the estimated change point.

Based on the results, assuming there is one change point in PM_{10} concentration in Fresno, Mono, and Monterey during the first half of 2023, the causal mechanism of PM_{10} in Fresno is likely to shift on May 8, 2023. Additionally, while the PM_{10} levels in Fresno and Monterey are not influenced by other counties, a causal link from Monterey to Mono has emerged after February 2, 2023.

Table 1: Change point detection in PM_{10} data with Causal-RuLSIF

Causal-RuLSIF			
X	\tilde{T}_c^j	$\{\widehat{\text{PA}}_k\}_{k \in [2]}$: parent sets before and after \tilde{T}_c^j	
\mathbf{X}^{Fr}	05/08/23	$\{X_{t-1}^{Fr}\};$	$\{X_{t-1}^{Fr}, X_{t-2}^{Fr}, X_{t-3}^{Fr}\}$
\mathbf{X}^{Mono}	02/01/23	$\{X_{t-1}^{\text{Mono}}\};$	$\{X_{t-2}^{\text{Mono}}, X_{t-1}^{\text{Mono}}, X_{t-3}^{\text{Mont}}\}$
\mathbf{X}^{Mont}	04/04/23	$\{X_{t-1}^{\text{Mont}}\};$	$\{X_{t-1}^{\text{Mont}}\}$

Without the ground truth and relevant knowledge about air pollution and other climate-related information, it is difficult to determine the significance of the case study results. We hope this real data application can offer insights for experts in other fields on detecting change points in the underlying causal mechanisms in practice.

6 Conclusion

In this paper, we introduced a novel change point detection algorithm, Causal-RuLSIF, to identify significant changes in causal mechanisms for discrete-valued time series data. By integrating a post-processing causal discovery stage with divergence estimation dynamically, our algorithm accurately detects when causal mechanism shifts occur without imposing constraints on the form of the shift. We provide a theoretical uncertainty analysis of the change point estimator. Our empirical evaluation confirms the consistency and robustness of the proposed algorithm. It is possible that the causal mechanism shift happens slowly over a short time period. It would be interesting to extend our approach to handle such smooth changes.

References

- Sofiane Brahim-Belhouari and Amine Bermak. Gaussian process for nonstationary time series prediction. *Computational Statistics & Data Analysis*, 47(4):705–712, 2004.
- Ian Cleland, Manhyung Han, Chris Nugent, Hosung Lee, Sally McClean, Shuai Zhang, and Sungyoung Lee. Evaluation of prompted annotation of activity data recorded from a smart phone. *Sensors*, 14(9):15861–15879, 2014.
- Richard J Radke, Srinivas Andra, Omar Al-Kofahi, and Badrinath Roysam. Image change detection algorithms: a systematic survey. *IEEE transactions on image processing*, 14(3):294–307, 2005.
- Makram Talih and Nicolas Hengartner. Structural learning with time-varying components: tracking the cross-section of financial time series. *Journal of the Royal Statistical Society Series B: Statistical Methodology*, 67(3):321–341, 2005.
- Makoto Yamada, Taiji Suzuki, Takafumi Kanamori, Hirotaka Hachiya, and Masashi Sugiyama. Relative density-ratio estimation for robust distribution comparison. *Neural computation*, 25(5):1324–1370, 2013.
- Song Liu, Makoto Yamada, Nigel Collier, and Masashi Sugiyama. Change-point detection in time-series data by relative density-ratio estimation. *Neural Networks*, 43:72–83, 2013.
- Zaid Harchaoui, Eric Moulines, and Francis Bach. Kernel change-point analysis. *Advances in neural information processing systems*, 21, 2008.
- Zaid Harchaoui, Félicien Vallet, Alexandre Lung-Yut-Fong, and Olivier Cappé. A regularized kernel-based approach to unsupervised audio segmentation. In *2009 IEEE international conference on acoustics, speech and signal processing*, pages 1665–1668. IEEE, 2009.
- Siddhartha Chib. Estimation and comparison of multiple change-point models. *Journal of econometrics*, 86(2):221–241, 1998.
- Jerome H Friedman and Lawrence C Rafsky. Multivariate generalizations of the wald-wolfowitz and smirnov two-sample tests. *The Annals of Statistics*, pages 697–717, 1979.
- Eamonn Keogh, Selina Chu, David Hart, and Michael Pazzani. An online algorithm for segmenting time series. In *Proceedings 2001 IEEE international conference on data mining*, pages 289–296. IEEE, 2001.
- Naoki Itoh and Jürgen Kurths. Change-point detection of climate time series by nonparametric method. In *Proceedings of the world congress on engineering and computer science*, volume 1, pages 445–448, 2010.
- Samaneh Aminikhanghahi and Diane J Cook. A survey of methods for time series change point detection. *Knowledge and information systems*, 51(2):339–367, 2017.
- Elena Saggioro, Jana de Wiljes, Marlene Kretschmer, and Jakob Runge. Reconstructing regime-dependent causal relationships from observational time series. *Chaos: An Interdisciplinary Journal of Nonlinear Science*, 30(11), 2020.
- Siqi Liu, Adam Wright, and Milos Hauskrecht. Change-point detection method for clinical decision support system rule monitoring. *Artificial intelligence in medicine*, 91:49–56, 2018.
- Judea Pearl. *Causality*. Cambridge university press, 2009.
- Jakob Runge. Causal network reconstruction from time series: From theoretical assumptions to practical estimation. *Chaos: An Interdisciplinary Journal of Nonlinear Science*, 28(7):075310, 2018.
- Jakob Runge, Peer Nowack, Marlene Kretschmer, Seth Flaxman, and Dino Sejdinovic. Detecting and quantifying causal associations in large nonlinear time series datasets. *Science advances*, 5(11):eaau4996, 2019.
- Mingming Gong, Kun Zhang, Bernhard Schoelkopf, Dacheng Tao, and Philipp Geiger. Discovering temporal causal relations from subsampled data. In *International Conference on Machine Learning*, pages 1898–1906. PMLR, 2015.
- Daniel Malinsky and Peter Spirtes. Learning the structure of a nonstationary vector autoregression. In *The 22nd International Conference on Artificial Intelligence and Statistics*, pages 2986–2994. PMLR, 2019.
- Biwei Huang, Kun Zhang, Mingming Gong, and Clark Glymour. Causal discovery and forecasting in nonstationary environments with state-space models. In *International conference on machine learning*, pages 2901–2910. PMLR, 2019.
- Biwei Huang, Kun Zhang, Jiji Zhang, Joseph D Ramsey, Ruben Sanchez-Romero, Clark Glymour, and Bernhard Schölkopf. Causal discovery from heterogeneous/nonstationary data. *J. Mach. Learn. Res.*, 21(89):1–53, 2020.
- Daigo Fujiwara, Kazuki Koyama, Keisuke Kiritoshi, Tomomi Okawachi, Tomonori Izumitani, and Shohei Shimizu. Causal discovery for non-stationary non-linear time series data using just-in-time modeling. In *2nd Conference on Causal Learning and Reasoning*, 2023.

- Shanyun Gao, Raghavendra Addanki, Tong Yu, Ryan A. Rossi, and Murat Kocaoglu. Causal discovery in semi-stationary time series. In *Thirty-seventh Conference on Neural Information Processing Systems*, 2023. URL <https://openreview.net/forum?id=dYeUvLUxBQ>.
- Lyudmila Yur'evna Vostrikova. Detecting “disorder” in multidimensional random processes. In *Doklady akademii nauk*, volume 259, pages 270–274. Russian Academy of Sciences, 1981.
- Malte Londschien, Peter Bühlmann, and Solt Kovács. Random forests for change point detection. *Journal of Machine Learning Research*, 24(216):1–45, 2023.
- Nicholas A James and David S Matteson. ecp: An r package for nonparametric multiple change point analysis of multivariate data. *arXiv preprint arXiv:1309.3295*, 2013.
- Wenyu Zhang, Nicholas A James, and David S Matteson. Pruning and nonparametric multiple change point detection. In *2017 IEEE international conference on data mining workshops (ICDMW)*, pages 288–295. IEEE, 2017.
- Judea Pearl. *Causality: models, reasoning, and inference*, 1980.
- David E Allen, Michael McAleer, Robert J Powell, and Abhay K Singh. Non-parametric multiple change point analysis of the global financial crisis. *Annals of Financial Economics*, 13(02):1850008, 2018.
- Hao Chen and Lynna Chu. Graph-based change-point analysis. *Annual Review of Statistics and Its Application*, 10: 475–499, 2023.

A Appendix

A.1 Preliminaries

A.1.1 Time Series Segments

In Fig. 1a), for \mathbf{X}^1 , $\text{SPA}(X_t^1) = \{X_{t-2}^1, X_{t-1}^1, X_{t-2}^2, X_{t-1}^3\}$. Assuming V is binary time series with $D = [0, 1]$, we have:

$$\Sigma^1 := \begin{matrix} & & X_{t-2}^1 & X_{t-1}^1 & X_{t-2}^2 & X_{t-1}^3 \\ \begin{matrix} 1 \\ 2 \\ 3 \\ \dots \\ s^{|\text{SPA}(X_t^j)|} \end{matrix} & \left[\begin{array}{cccc} 0 & 0 & 0 & 0 \\ 1 & 0 & 0 & 0 \\ 0 & 1 & 0 & 0 \\ \dots & \dots & \dots & \dots \\ 1 & 1 & 1 & 1 \end{array} \right] & \begin{matrix} \\ \\ \\ \\ s^{|\text{SPA}(X_t^j)|} \times |\text{SPA}(X_t^j)| \end{matrix} \end{matrix} \quad (17)$$

With $s = |D| = 2$ and $|\text{SPA}(X_t^j)| = 4$, there are $16 = 2^4$ configurations of $\text{SPA}(X_t^j)$. Hence there are 16 Time Series Segments of \mathbf{X}^1 . More specifically, $X^1(1) := \{X_t^j : t \in [\tau_{\max} + 1, T], \text{pa}(X_t^j) = [0, 0, 0, 0]\}$, $X^1(2) := \{X_t^j : t \in [\tau_{\max} + 1, T], \text{pa}(X_t^j) = [0, 1, 0, 0]\}$ and so on. For \mathbf{X}^3 , $\text{SPA}(X_t^3) = \{X_{t-3}^2, X_{t-1}^2, X_{t-1}^3\}$ and hence there are total $2^3 = 8$ configurations. Fig.1b) shows the construction of $X^3(1)$ and Fig.1c) illustrates 8 total Time Series Segments of \mathbf{X}^3 .

A.1.2 RuLSIF: Robust Distribution Comparison

Given two distributions $p(\cdot)$ and $p'(\cdot)$ defined over the same support, there exists many metrics measuring the distance between them. In Yamada et al. [2013], proposed a method named RuLSIF, with an α -relative divergence estimation $r_\alpha(x)$ and a corresponding metric, α -relative Pearson Divergence PE_α defined as following:

$$r_\alpha(x) := \frac{p(x)}{(1 - \alpha)p(x) + \alpha p'(x)} := \frac{p(x)}{q_\alpha(x)} \quad (18)$$

$$PE_\alpha := \frac{1}{2} \mathbb{E}_{x \sim q_\alpha} [(r_\alpha(x) - 1)^2] \quad (19)$$

where α is a parameter used to bound the value of $r_\alpha(x)$. With IID samples, we can obtain a direct density-ratio estimator $\hat{r}_\alpha(x)$ using a kernel function, by minimizing a squared loss function. The estimator has been proven to have a non-parametric convergence speed. In Liu et al. [2013], the method was applied to tackle the change point detection problem in time series using sliding windows. By dividing the time series into retrospective segments, a sequence of RuLSIF measurements is obtained by assessing the distribution divergence between samples from two consecutive segments. Peaks in the divergence score PE_α can indicate change points within the joint distribution. The retrospective segments in Liu et al. [2013] are high-dimensional, even for univariate time series V .

In our proposed method, we also utilize sliding windows. However, since the focus shifts from the joint distribution to the causal mechanism, we do not construct high-dimensional retrospective segments from V . Instead, we create one-dimensional consecutive segments on the Time Series Segments for each $\mathbf{X}^j \subseteq V$. This approach avoids the Curse of dimensionality and enhances the method's robustness to the hyperparameters in the kernel functions, as will be verified in the experiment section.

Since we apply the RuLSIF method to the Time Series Segments, the samples are IID. The distributions that need to be compared are formalized as follows:

$$p(X_{t_1}^j | \text{spa}(X_{t_1}^j) = \Sigma_\Lambda) \text{ vs } p(X_{t_2}^j | \text{spa}(X_{t_2}^j) = \Sigma_\Lambda) \quad (20)$$

where $\Lambda \in [s^{|\text{SPA}(X_t^j)|}]$, $t_1 < T_c$ and $t_2 \geq T_c$.

To simplify matters, we use $p(x)$ to denote $p(X_{t_1}^j | \text{spa}(X_{t_1}^j) = \Sigma_\Lambda)$ and $p'(x)$ represent $p(X_{t_2}^j | \text{spa}(X_{t_2}^j) = \Sigma_\Lambda)$ in the rest of the paper.

Fig.4 provides a toy example demonstrating how the sliding window operates on Time Series Segments. From each segment, a series of PE scores is obtained using two sets of samples from the two halves of the sliding windows. Denote W_i as the i th window, with W_i^1 representing the first half and W_i^2 representing the second half.

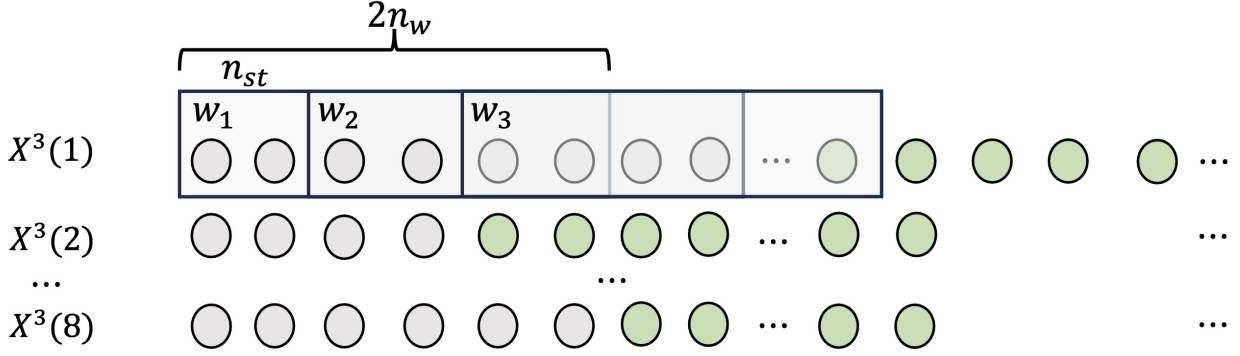


Figure 4: 8 Time Series Segments obtained from Fig.1 for \mathbf{X}^3 . This toy example illustrates the sliding windows with n_w, n_{st} for $\{X^3(\Lambda)\}_{\Lambda \in [8]}$

In the i th sliding window containing one change point, without loss of generality, assume that the change point is within the second half, W_i^2 , of the window. Thus, while the samples in W_i^1 come from $p(x)$, the samples in W_i^2 come from a mixture distribution $(1 - \beta_i)p(x) + \beta_i p'(x)$, where β_i is the proportion of samples from $p'(x)$ within W_i^2 . Note that β_i is an unknown parameter, while i is the known window index. Therefore, it is more accurate to denote the divergence score for the i th window as $PE_{\alpha\beta_i}$. To clarify, we will use $PE_{\alpha\beta_i}$ instead. By replacing $p'(x)$ with $(1 - \beta_i)p(x) + \beta_i p'(x)$ in Eq.18, we obtain the $\alpha\beta_i$ -relative divergence estimation $r_{\alpha\beta_i}(x)$ and the $\alpha\beta_i$ -relative Pearson Divergence for the i th window

$$r_{\alpha\beta_i}(x) := \frac{p(x)}{(1 - \alpha\beta_i)p(x) + \alpha\beta_i p'(x)} := \frac{p(x)}{q_{\alpha\beta_i}(x)} \quad (21)$$

$$PE_{\alpha\beta_i} := \frac{1}{2} \mathbb{E}_{x \sim q_{\alpha\beta_i}} [(r_{\alpha\beta_i}(x) - 1)^2] \quad (22)$$

A.1.3 Assumptions

- A1. Sufficiency:** There are no unobserved confounders.
- A2. Causal Markov Condition:** Each variable X is independent of all its non-descendants, given its parents $\text{PA}(X)$ in \mathcal{G} .
- A3. Faithfulness Condition Pearl [1980]:** Let P be a probability distribution generated by \mathcal{G} . $\langle \mathcal{G}, P \rangle$ satisfies the Faithfulness Condition if and only if every conditional independence relation true in P is entailed by the Causal Markov Condition applied to \mathcal{G} .
- A4. No Contemporaneous Causal Effects:** Edges between variables at the same time are not allowed.
- A5. Temporal Priority:** Causal relations always point from the past to the future.
- A6. Boundary Separation Assumption:** There must be a minimum buffer period at both the beginning and the end of the time series where change points cannot be detected. More specifically, the change point for each time series $\mathbf{X}^j \in V$ cannot occur within the specified window size n_w .
- A7. One change point per component time series:** $\forall j, c^j = 1$, that is, each time series $\mathbf{X}^j \in V$ has only one change point.
- A8. Minimum Pearson Divergence:** For each $\mathbf{X}^j \subsetneq V$, there should exist a window W^i satisfying $PE_{\alpha\beta_i} > \frac{\|r_{\alpha\beta_i}\|_{\infty}^2}{4} + \frac{(1 - \alpha\beta_i)^2 \|r_{\alpha\beta_i}\|_{\infty}^4}{16} + \frac{\alpha^2 \beta_i^2 \|r_{\alpha\beta_i}\|_{\infty}^4}{16}$ in at least one Time Series Segments $X^j(\Lambda)$.

Assumptions **A1-A5** are conventional and commonly employed in causal discovery methods for time series data. Our approach requires specific Assumptions **A6-A8** to be in place. To clarify, assumption **A6** is essential because our algorithm utilizes a series of sliding windows to obtain the divergence score by measuring the first half and the second half of the samples within each window. If the change point is too close to the beginning or end of the time series, the divergence score will not be significant enough to be detected. Assumption **A7** is required since the sliding windows are not directly applied on the original time series. Instead, multiple sub-time series are created and hence it is hard to impose the constraint on the minimum distance among multiple change points, such as in Harchaoui et al. [2009],

Allen et al. [2018] and Chen and Chu [2023]. Assumption **A8** is necessary for the proof, as it guarantees a significant difference between two distinct causal mechanisms. This assumption is crucial because detecting the change point successfully becomes highly unlikely if the two causal mechanisms are extremely similar.

A.2 Theoretical Guarantees

Theorem A.1 ensures that in the initial step of our algorithm, a superset of the true union parent set $\text{SPA}X_t^j$ can be obtained for all $j \in [n]$. This guarantees the correct construction of Time Series Segments $X^j(\Lambda)$, with IID samples. Theorem A.2 establishes that if the window W_i contains samples from a single conditional distribution, the estimated relative Pearson Divergence $\widehat{PE}_{\alpha\beta_i}$ is close to zero with high probability. Lemma A.3 states that, as n_w increases, the estimated relative Pearson Divergence will be close to the true relative Pearson Divergence up to some constant with high probability. Lemma A.4 proves that the Pearson Divergence will achieve the maximum if all the samples in the first half window are from p and the samples in the second half window are from p' . Theorem A.5 establishes a confidence interval for the change point estimator \widehat{T}_c^j .

Theorem A.1. *Let $\text{SPA}(X_t^j)$ denote the union parent set of X_t^j and $\widehat{\text{SPA}}(X_t^j)$ denote the estimated union parent set obtained from PCMC algorithm on time series \mathbf{X}^j with a Causal-shift causal mechanism, and the change point T_c^j satisfies $T_c^j = \frac{T}{2}$. Under assumptions **A1-A5,A7** and with an oracle (infinite sample size limit), we have that:*

$$\text{SPA}(X_t^j) \subseteq \widehat{\text{SPA}}(X_t^j) \quad (23)$$

Theorem A.1 asserts that when samples are balanced, with half originating from one causal mechanism and the remaining half from another, the estimated union parent set encompasses the true union parent set.

Proof. The proof follows the same logic as the Lemma 3.2 and 3.3 in Gao et al. [2023]. In the semi-stationary SCM, the samples are from multiple causal mechanisms and due to periodicity, heterogeneous samples from different causal mechanisms are balanced. However, in the causal-shift SCM, as per Assumption **A7**, there are only two causal mechanisms, and the samples are inherently unbalanced without specific clarification. With additional assumption $T_c^j = \frac{T}{2}$, we can draw the same conclusion as in Gao et al. [2023]. \square

Note that $\widehat{PE}_{\alpha\beta_i}^{j,\Lambda}$ series with parameter α and window index i is a function of n_w, n_{st} , time series index j and Time Series Segments index Λ . For simplicity, we use $\widehat{PE}_{\alpha\beta_i}$ instead of $\widehat{PE}_{\alpha\beta_i}^{j,\Lambda}(n_w, n_{st})$ in the next section. Furthermore, we need to emphasize that T_{sub} is not the length of V but the length of the specific Time Series Segments.

Theorem A.2. *Let $\widehat{PE}_{\alpha\beta_i}$ be the estimated PE series for one Time Series Segments $X^j(\Lambda) \subsetneq \mathbf{X}^j \subsetneq V$. Under assumption **A6-A7**, we have that $\forall i \in \{i : in_{st} + 2n_w - 1 < T_c\}$*

$$P(\max_i |\widehat{PE}_{\alpha\beta_i}| < o_p(1)) > 1 - \frac{a_w - 2}{b_{st} \log T_{\text{sub}}} - \frac{a_w}{T_{\text{sub}}} \quad (24)$$

where $b_{st} = \lfloor \frac{\log T_{\text{sub}}}{n_{st}} \rfloor$ and $a_w = \lceil \frac{T_{\text{sub}}}{n_w} \rceil$.

The window index i satisfying $in_{st} + 2n_w - 1 < T_c$ guarantees that all the samples in W_i are collected from the same distribution. Theorem A.2 states that the maximum estimated PE series obtained from such windows are bounded by any positive constant with probability $1 - \frac{a_w - 2}{b_{st} \log T_{\text{sub}}} - \frac{a_w}{T_{\text{sub}}}$ if n_w are larger than some threshold. In other words, $\forall k > 0, \exists N$ such that $\forall n_w \geq N$:

$$P(\max_i |\widehat{PE}_{\alpha\beta_i}| < k) = 1 - \frac{a_w - 2}{b_{st} \log T_{\text{sub}}} - \frac{a_w}{T_{\text{sub}}} \quad (25)$$

Proof. $\forall i \in \{i : in_{st} + 2n_w - 1 < T_c\}$, the asymptotic expectation and variance of $\widehat{PE}_{\alpha\beta_i}$ is given by:

$$\mathbb{E}(\widehat{PE}_{\alpha\beta_i}) = PE_{\alpha\beta_i} + o_p\left(\frac{1}{\sqrt{n_w}}\right) \quad (26)$$

$$= o_p\left(\frac{1}{\sqrt{n_w}}\right) \quad (27)$$

$$\mathbb{V}(\widehat{PE}_{\alpha\beta_i}) = o_p\left(\frac{1}{n_w}\right) \quad (28)$$

The proof of the asymptotic expectation and variance can be found in Section B of Yamada et al. [2013]. By Chebyshev's inequality, we have:

$$p(|\widehat{PE}_{\alpha\beta_i}| > ko_p(\frac{1}{\sqrt{n_w}})) \leq \frac{1}{k^2} \quad (29)$$

Denote A_i as the event that $|\widehat{PE}_{\alpha\beta_i}| > ko_p(\frac{1}{\sqrt{n_w}})$. By Boole's inequality, the union bound of the series for $i \in \{i : in_{st} + 2n_w - 1 < Tc\}$ is given by:

$$P(\cup_{i=0}^{\lfloor \frac{|T_{sub}|-2n_w}{n_{st}} \rfloor + 1} A_i) \leq \sum_{i=0}^{\lfloor \frac{|T_{sub}|-2n_w}{n_{st}} \rfloor + 1} p(A_i) \leq \frac{\lfloor \frac{|T_{sub}|-2n_w}{n_{st}} \rfloor + 1}{k^2} \quad (30)$$

$$P(\cap_{i=0}^{\lfloor \frac{|T_{sub}|-2n_w}{n_{st}} \rfloor + 1} A_i^c) \geq 1 - \frac{\lfloor \frac{|T_{sub}|-2n_w}{n_{st}} \rfloor + 1}{k^2} \quad (31)$$

That is, the probability that the maximum value of $\{\widehat{PE}_{\alpha\beta_i}\}_{i=0}^{in_{st}+2n_w-1 < Tc^j}$ is less than $ko_p(\frac{1}{\sqrt{n_w}})$ is larger than $1 - \frac{\lfloor \frac{|T_{sub}|-2n_w}{n_{st}} \rfloor + 1}{k^2}$. The same results hold for $\forall i \in \{i : in_{st} \geq Tc\}$.

Let $n_{st} = b_{st} \log T_{sub}$, $k = \sqrt{n_w}$ and make n_w a proportion of T_{sub} , which can be denoted by $\frac{T}{a_w}$ where b_{st} and a_s are both constants.

We have:

$$P(\cap_{i=0}^{\lfloor \frac{|T_{sub}|-2T}{b_{st} \log T} \rfloor + 1} A_i^c) > 1 - \frac{a_w - 2}{b_{st} \log T} - \frac{a_w}{T} \quad (32)$$

In other words, the likelihood that the maximum $PE_{\alpha,i}$, encompassing all samples before T_c^j or after T_c^j , is less than $\sqrt{n_w}o(\sqrt{n_w})$ is greater than $1 - \frac{a_w-2}{b_{st} \log T} - \frac{a_w}{T}$. More specifically:

$$P(\max_i |\widehat{PE}_{\alpha\beta_i}| < \sqrt{n_w}o_p(\frac{1}{\sqrt{n_w}})) > 1 - \frac{a_w - 2}{b_{st} \log T} - \frac{a_w}{T} \quad (33)$$

□

Lemma A.3. Let $\widehat{PE}_{\alpha\beta_i}$ be the estimated PE series for one Time Series Segments $X^j(\Lambda) \subsetneq \mathbf{X}^j \subsetneq V$. Under assumption A6-A7, we have that $\forall i \in \{i : T_c^j < in_{st} + 2n_w - 1 < T_c^j + n_w\}$,

$$p(PE_{\alpha\beta_i} - c_i - (\sqrt{n_w} - 1)o_p(\frac{1}{\sqrt{n_w}})) \leq \widehat{PE}_{\alpha\beta_i} \quad (34)$$

$$\leq PE_{\alpha\beta_i} + c_i + (\sqrt{n_w} + 1)o_p(\frac{1}{\sqrt{n_w}})) > 1 - \frac{1}{n_w} \quad (35)$$

where $c_i := \frac{\|r_{\alpha\beta_i}\|_\infty^2}{4} + \frac{(1-\alpha\beta_i)^2 \|r_{\alpha\beta_i}\|_\infty^4}{16} + \frac{\alpha^2 \beta_i^2 \|r_{\alpha\beta_i}\|_\infty^4}{16}$.

The window index i satisfying $T_c^j < in_{st} + 2n_w - 1 < T_c^j + n_w$ guarantees that all the samples in W_i^1 are collected from $p(x)$ and samples in W_i^2 are from a mixture distribution $(1 - \beta_i)p(x) + \beta_i p'(x)$. Lemma A.3 states that the estimated error between the estimated PE series and the true PE value is smaller than a constant with probability $1 - \frac{1}{n_w}$ if n_w are larger than some threshold. In other words, $\forall k > 0, \exists N$ such that $\forall n_w \geq N$:

$$P(|\widehat{PE}_{\alpha\beta_i} - PE_{\alpha\beta_i}| < k + c_i) = 1 - \frac{1}{n_w} \quad (36)$$

Proof. $\forall i \in \{i : T_c < in_s + 2n_w - 1 < T_c + n_w\}$, the asymptotic expectation and variance of $\widehat{PE}_{\alpha\beta_i}$ is given by:

$$\mathbb{E}(\widehat{PE}_{\alpha\beta_i}) = PE_{\alpha\beta_i} + o_p(\frac{1}{\sqrt{n_w}}) \quad (37)$$

$$\mathbb{V}(\widehat{PE}_{\alpha\beta_i}) = \frac{\|r_{\alpha\beta_i}\|_\infty^2}{4n_w} + \frac{(1 - \alpha\beta_i)^2 \|r_{\alpha\beta_i}\|_\infty^4}{16n_w} + \frac{\alpha^2 \beta_i^2 \|r_{\alpha\beta_i}\|_\infty^4}{16n_w} + o_p(\frac{1}{n_w}). \quad (38)$$

For simplicity, let $\sigma_i^2 := \frac{\|r_{\alpha\beta_i}\|_\infty^2}{4n_w} + \frac{(1-\alpha\beta_i)^2\|r_{\alpha\beta_i}\|_\infty^4}{16n_{st}} + \frac{\alpha^2\beta_i^2\|r_{\alpha\beta_i}\|_\infty^4}{16n_{st}}$.

By Chebyshev's inequality, we have:

$$p(|\widehat{PE}_{\alpha\beta_i} - PE_{\alpha\beta_i} - o_p(\frac{1}{\sqrt{n_w}})| > k(\sigma_i + o_p(\frac{1}{\sqrt{n_w}}))) \leq \frac{1}{k^2} \quad (39)$$

$$p(|\widehat{PE}_{\alpha\beta_i} - PE_{\alpha\beta_i} - o_p(\frac{1}{\sqrt{n_w}})| \leq k(\sigma_i + o_p(\frac{1}{\sqrt{n_w}}))) > 1 - \frac{1}{k^2} \quad (40)$$

Hence we have:

$$p(PE_{\alpha\beta_i} - k\sigma_i - (k-1)o_p(\frac{1}{\sqrt{n_w}}) \leq \widehat{PE}_{\alpha\beta_i} \leq PE_{\alpha\beta_i} + k\sigma_i + (k+1)o_p(\frac{1}{\sqrt{n_w}})) > 1 - \frac{1}{k^2} \quad (41)$$

Let $k = \sqrt{n_w}$ and make n_w a proportion of T , which can be denoted by $\frac{T}{a_w}$ where a_s is a constant.

We have:

$$p(PE_{\alpha\beta_i} - c_i - (\sqrt{n_w} - 1)o_p(\frac{1}{\sqrt{n_w}}) \leq \widehat{PE}_{\alpha\beta_i} \leq PE_{\alpha\beta_i} + c_i + (\sqrt{n_w} + 1)o_p(\frac{1}{\sqrt{n_w}})) \quad (42)$$

$$> 1 - \frac{1}{n_w} \quad (43)$$

where $c_i^2 := \frac{\|r_{\alpha\beta_i}\|_\infty^2}{4} + \frac{(1-\alpha\beta_i)^2\|r_{\alpha\beta_i}\|_\infty^4}{16} + \frac{\alpha^2\beta_i^2\|r_{\alpha\beta_i}\|_\infty^4}{16}$.

□

Since we only discuss the discrete distribution, therefore we can assume that there are k realizations of any variable X_t^j from 1 to k . For simplicity, we denote $p(x = k)$ as p_h and $p'(x = k)$ as p'_h .

Lemma A.4. *Let $PE_{\alpha\beta_i}$ be the estimated PE series for one Time Series Segments $X^j(\Lambda) \subsetneq \mathbf{X}^j \subsetneq V$. Under assumption A6-A7, we have that $\forall i \in \{i : T_c^j < in_{st} + 2n_w - 1 < T_c^j + n_w\}$,*

- $PE_{\alpha\beta_i} > 0$
- $PE_{\alpha\beta_i}$ is a monotonically increasing function regarding i (or β_i).
- $\max PE_{\alpha\beta_i} = \frac{1}{2} \sum_{h=1}^k \frac{p_h^2}{(1-\alpha\beta^*)p_h + \alpha\beta^*p'_h} - \frac{1}{2}$ where β^* is the largest proportion of samples from $p'(x)$ over those second windows $\{W_i^2\}_{i:T_c^j < in_{st} + 2n_w - 1 < T_c^j + n_w}$. For appropriate n_w and n_{st} , $\max PE_{\alpha\beta_i}$ can achieve the maximum when all samples of W_i^1 are from $p(x)$ and all samples of W_i^2 are from $p'(x)$, that is, $\max_i \beta_i = 1$.

Lemma A.4 suggests that the true PE series derived from the sequence of sliding windows is a monotonically increasing function with respect to β_i if the samples in the second half of the sliding windows are from a mixture distribution, indicating that the change point is located within the second half of the sliding windows. Similarly, employing the same reasoning, the true PE series becomes a monotonically decreasing function with respect to β_i if the samples in the first half of the windows are from a mixture distribution, that is, $i \in \{i : T_c^j + n_w < in_{st} + 2n_w - 1 < T_c^j + 2n_w\}$. Here, β_i represents the proportion of samples from $p(x)$ over the first half windows.

Proof. Treat $PE_{\alpha\beta_i}$ as a function of $\alpha := \alpha\beta_i$.

$$PE_{\alpha\beta_i} = \frac{1}{2} \mathbb{E}_{p(x)}[r_{\alpha\beta_i}(x)] - \frac{1}{2} \quad (44)$$

$$= \frac{1}{2} \sum_{h=1}^k \frac{p_h}{(1-\alpha)p_h + \alpha p'_h} p_h - \frac{1}{2} \quad (45)$$

$$= \frac{1}{2} \sum_{h=1}^k \frac{p_h}{1 + (\frac{p'_h}{p_h} - 1)\alpha} - \frac{1}{2} \quad (46)$$

We have:

$$f(\alpha) := \sum_{h=1}^k \frac{p_h}{1 + (\frac{p'_h}{p_h} - 1)\alpha} \quad (47)$$

$$f'(\alpha) = \sum_{h=1}^k \frac{-p_h(\frac{p'_h}{p_h} - 1)}{(1 + (\frac{p'_h}{p_h} - 1)\alpha)^2} \quad (48)$$

$$f''(\alpha) = \sum_{h=1}^k \frac{2p_h(\frac{p'_h}{p_h} - 1)^2}{(1 + (\frac{p'_h}{p_h} - 1)\alpha)^3} \quad (49)$$

Since $\frac{p'_h}{p_h} > 0$ and $0 \leq \alpha \leq 1$, we have $1 + (\frac{p'_h}{p_h} - 1)\alpha > 0$ for any $j \in [k]$, hence $f''(\alpha) > 0$, leading to an increasing function $f'(\alpha)$.

$$f'(\alpha) \geq f'(0) = \sum_{h=1}^k (p_h - p'_h) = 0 \quad (50)$$

Hence $f(\alpha)$ is an increasing function in terms of α and

$$f(\alpha) \geq f(0) = \sum_{h=1}^k p_h = 1, \text{ with } \alpha \in [0, 1] \quad (51)$$

□

Theorem A.5. Let $\widehat{PE}_{\alpha\beta_i}$ be the estimated PE series for one Time Series Segments $X^j(\Lambda) \subseteq \mathbf{X}^j \subseteq V$ and T_c^j denote the true change point in this Time Series Segments. \widehat{T}_c^j denotes the estimator of T_c^j obtained by:

$$\widehat{T}_c^j = \arg_i \max \widehat{PE}_{\alpha\beta_i} \quad (52)$$

Under assumption **A6-A8**, we have that given large enough n_w , $\forall i \in [\tau_{max} + 1, T]$

$$P(|\widehat{T}_c^j - T_c^j| < 2n_w) > (1 - \frac{a_w - 2}{b_{st} \log T_{sub}} - \frac{a_w}{T_{sub}})(1 - \frac{1}{n_w}) \quad (53)$$

where $b_{st} = \lfloor \frac{\log T_{sub}}{n_{st}} \rfloor$ and $a_w = \lceil \frac{T_{sub}}{n_w} \rceil$.

Proof. From Theorem A.2, $\forall k_1 > 0, \exists N_1$ such that $\forall n_w \geq N_1$, we have $\forall i_1 \in \{i_1 : i_1 n_{st} + 2n_w - 1 < T_c^j\}$:

$$P(\max_{i_1} |\widehat{PE}_{\alpha\beta_{i_1}}| < k_1) > 1 - \frac{a_w - 2}{b_{st} \log T_{sub}} - \frac{a_w}{T_{sub}} \quad (54)$$

From Lemma A.3, $\forall k_2 > 0, \exists N_2$ such that $\forall n_w \geq N_2$, we have $\forall i_2 \in \{i_2 : T_c^j < i_2 n_{st} + 2n_w - 1 < T_c^j + n_w\}$:

$$P(|\widehat{PE}_{\alpha\beta_{i_2}} - PE_{\alpha\beta_{i_2}}| < k_2 + c_{i_2}) = 1 - \frac{1}{n_w} \quad (55)$$

With Assumption **A8**, $\exists i_2$ such that $PE_{\alpha\beta_{i_2}} > c_{i_2}$, hence $\exists k_1, k_2 > 0$:

$$PE_{\alpha\beta_{i_2}} \geq c_{i_2} + k_2 + k_1 \quad (56)$$

Hence we can replace k_1 with $PE_{\alpha\beta_{i_2}} - c_{i_2} - k_2$ in Eq.54 and then we have:

$$P(\max_{i_1} |\widehat{PE}_{\alpha\beta_{i_1}}| < PE_{\alpha\beta_{i_2}} - c_{i_2} - k_2) > 1 - \frac{a_w - 2}{b_{st} \log T_{sub}} - \frac{a_w}{T_{sub}} \quad (57)$$

From Lemma A.3, we have:

$$PE_{\alpha\beta_{i_2}} - k_2 - c_{i_2} < \widehat{PE}_{\alpha\beta_{i_2}} < PE_{\alpha\beta_{i_2}} + k_2 + c_{i_2} \quad (58)$$

holds with probability $1 - \frac{1}{n_w}$.

As samples in W_{i_1} and W_{i_2} are IID, the events in Eq.57 and Eq.58 are independent, resulting in:

$$P(\max_{i_1} |\widehat{PE}_{\alpha\beta_{i_1}}| < \widehat{PE}_{\alpha\beta_{i_2}}) > (1 - \frac{a_w - 2}{b_{st} \log T_{sub}} - \frac{a_w}{T_{sub}})(1 - \frac{1}{n_w}) \quad (59)$$

for $\forall i_1 \in \{i_1 : i_1 n_{st} + 2n_w - 1 < T_c\}$ and $\exists i_2 \in \{i : T_c^j < i_2 n_{st} + 2n_w - 1 < T_c^j + n_w\}$.

From Lemma A.4, we know that $\exists \beta^*$ such that $PE_{\alpha\beta^*} = \max PE_{\alpha\beta_{i_2}}$. Denote $i_2^* = \arg_{i_2} \max PE_{\alpha\beta_{i_2}}$.

Since $PE_{\alpha\beta_{i_2}}$ is a monotonically increasing function regarding β_i , then the true change point T_c must satisfying:

$$PE_{\alpha\beta_{T_c}} \geq PE_{\alpha\beta^*} \geq \widehat{PE}_{\alpha\beta_{i_2}}, \quad (60)$$

$\forall i_2 \in \{i : T_c^j < i_2 n_{st} + 2n_w - 1 < T_c^j + n_w\}$ as n_{st} , n_w and T has jointly determined β_i . The proof for situations that $\{i_1 : i_1 n_{st} \geq T_c\}$ and $i_2 \in \{i : T_c^j + n_w < i n_{st} + 2n_w - 1 < T_c^j + 2n_w\}$ follows the same logic.

With Eq.60, we finally have:

$$P(|\widehat{T}_c^j - T_c^j| < 2n_w) > (1 - \frac{a_w - 2}{b_{st} \log T_{sub}} - \frac{a_w}{T_{sub}})(1 - \frac{1}{n_w}) \quad (61)$$

□

B Generate Binary-valued Time Series

The generation process have three steps.

1. Determine time series length T , number of time series n of the multivariate time series, data domain D , maximum time lag τ_{max} . Randomly generate T_c^j , $j \in [n]$, satisfying Definition 3.2 and Assumption **A6-A7**. Additionally, in order to guarantee enough samples in each time series segment, we also control the size of the union parent set, that is, $|\text{SPAX}_t^j|$.

With n , τ_{max} and the number of change points for each component time series c^j , one binary edge array with dimension $[n, c^j + 1, n, \tau_{max} + 1]$ is randomly generated, where the first n denotes the index of parent variable, c^j denotes the number of change point, the second n represents the index of target variable (child) and $\tau_{max} + 1$ denotes the time lag. With Assumption **A7**, $c^j = 1$ for all $j \in [n]$. 1 in this binary edge array means that there is an edge from the parent variable to the child variable with the corresponding time lag; 0 means that there is no cause-effect between two corresponding variables.

For soft mechanism change, the parent set remains the same before and after the change point, hence the binary edge array satisfies $[:, 0, :, :] =[:, 1, :, :]$. For hard mechanism change, the binary edge array must satisfy $[:, 0, :, :] \neq[:, 1, :, :]$.

2. With the randomly generated binary edge array controlled by $|\text{SPAX}_t^j|$, a full causal graph for this n -variate time series is obtained. Given this edge array and data domain D , parent configuration matrices $\{\Sigma^j\}_{j \in [n]}$ are obtained. Corresponding to $\{\Sigma^j\}_{j \in [n]}$, conditional probability tables (CPTs) are randomly generated. For instance, in Fig. 1, \mathbf{X} has a Σ^j with dimension 16×4 , resulting in 16 conditional distributions of X_t^1 given its specific parent configuration.
3. Fill the starting points $\{X_{t \leq \tau_{max}}^j\}_{j \in [n]}$ with randomly generated binary data. Starting from time point $t > \tau_{max}$, generate vector \mathbf{X}_t over time according to the CPTs, until t achieves T .

Please note that since our algorithm can be extended to handle multiple change points, the generation process can also be easily extended to accommodate such settings.

C Additional Experiments

From Fig.5(a) and Fig.5(b), it's apparent that a large n_w may affect the performance of Causal-RuLSIF. This issue still stems from sample efficiency. The total number of windows for a specific time series segment $X^j(\Lambda)$ is given by $\lfloor \frac{|T_{sub}| - 2n_w}{n_{st}} \rfloor + 1$, where $T_{sub} = |X^j(\Lambda)|$. Increasing n_w decreases the total number of windows, resulting in less information collected, as smaller n_w is sufficient to estimate PE scores with kernel functions.

As demonstrated in Fig.6(a) and Fig.6(b), the performance of Causal-RuLSIF remains consistent regardless of the distance between the change points T_c^1 of \mathbf{X}^1 and T_c^2 of \mathbf{X}^2 .

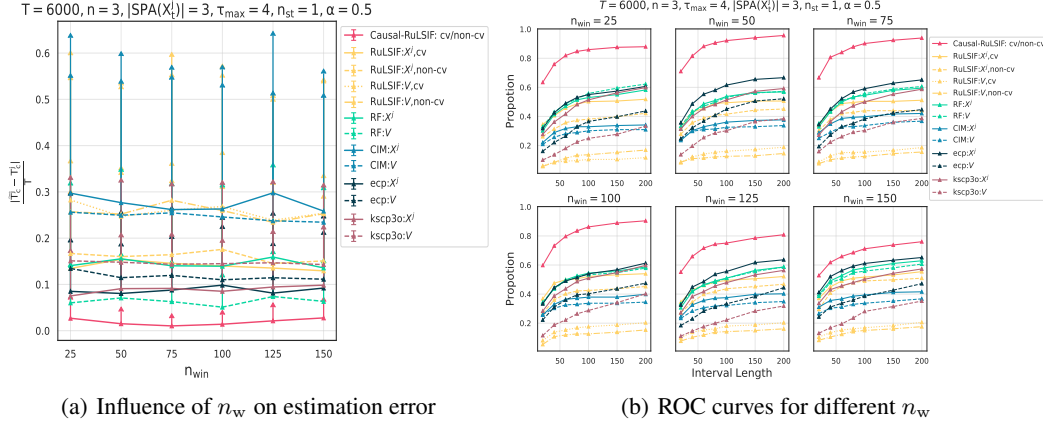


Figure 5: Causal-RuLSIF is tested on 3-multivariate time series with $T = 6000$, $\tau_{\max} = 4$, $|\text{SPA}(X_t^j)| = 3$, $n_{\text{st}} = 1$ with *soft mechanism change*. Every line with a different color corresponds to a different algorithm and different linestyle corresponds to a different setting. X^j in the legend means the algorithm is applied to each component time series while V means the algorithm is used for the whole n -variate time series V . Every marker corresponds to the average accuracy rate or average running time over 100 random trials. The error bar represents the standard error for the averaged statistics. a) Influence of n_w on estimation error $\frac{|\hat{T}_c^j - T_c^j|}{T}$. b) ROC curves for different n_w .

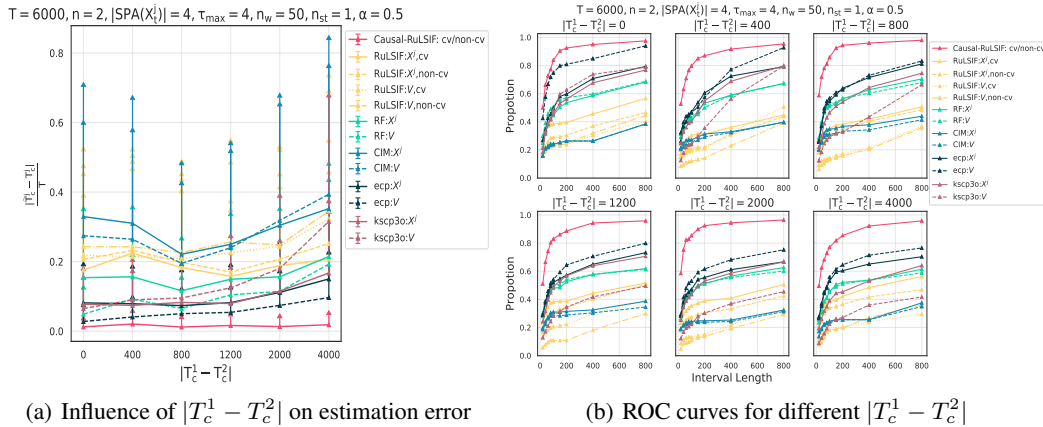


Figure 6: Causal-RuLSIF is tested on 3-multivariate time series with $T = 6000$, $\tau_{\max} = 4$, $|\text{SPA}(X_t^j)| = 3$, $n_w = 50$, $n_{\text{st}} = 1$ with *soft mechanism change*. Every line with a different color corresponds to a different algorithm and different linestyle corresponds to a different setting. X^j in the legend means the algorithm is applied to each component time series while V means the algorithm is used for the whole n -variate time series V . Every marker corresponds to the average accuracy rate or average running time over 100 random trials. The error bar represents the standard error for the averaged statistics. a) Influence of $|T_c^1 - T_c^2|$ on estimation error $\frac{|\hat{T}_c^j - T_c^j|}{T}$. b) ROC curves for different $|T_c^1 - T_c^2|$.

Fig. 7 shows the running time needed for each algorithm in seconds. Cross-validation techniques is time-consuming. It is beneficial that cross-validation is not needed for binary time series data for Causal-ReLSIF. Additionally, in order to have a better illustration of implementing dynamic divergence measurement on Time Series Segments, we have conducted experiments on randomly generated binary time series and plot the PE divergence series obtained from the Time Series Segments.

The estimated PE divergence series shown in Fig. 8 for one Time Series Segment verifies Theorem 4.1, Lemma A.4 and Theorem 4.2 empirically. For window index i smaller than around 500 or larger than around 900, \widehat{PE}_i score is very close to zero. For window index i between 500 and 900, \widehat{PE}_i first monotonically increases and then monotonically decreases over the window index i and the maximum value is achieved at $\widehat{T}_c = 864$, which equals to the true change

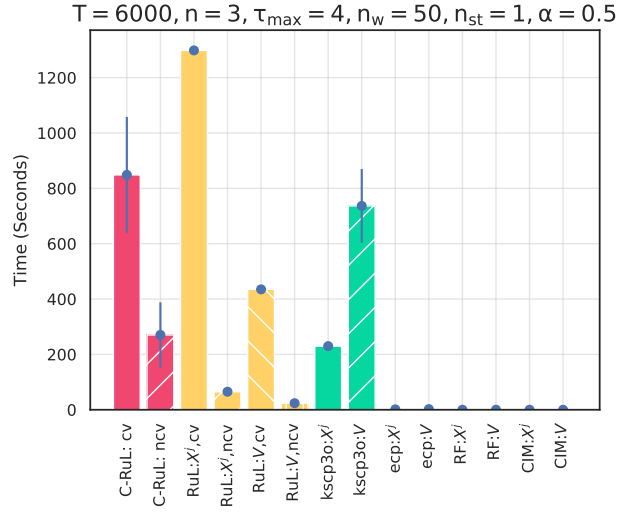


Figure 7: Runtime (in sec.) for algorithms

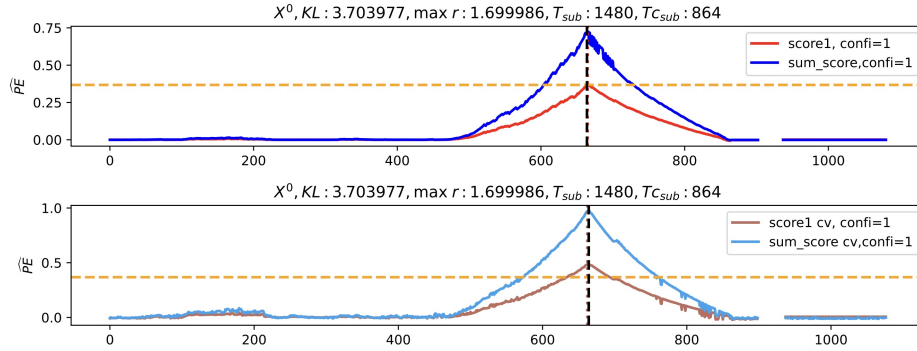


Figure 8: One estimated PE divergence series obtained on one Time Series Segment.

point in this Time Series Segment. Furthermore, the maximum of the PE score line is equal to the true PE value, which is denoted by the dashed orange horizontal line.